THE EUROPEAN
PHYSICAL JOURNAL A

Low-x QCD physics from RHIC and HERA to the LHC

D. d'Enterria[a]

CERN, PH-EP, CH-1211 Geneva 23, Switzerland

Abstract. We present a summary of the physics of gluon saturation and non-linear QCD evolution at small values of the parton momentum fraction x in the proton and nucleus in the context of recent experimental results at HERA and RHIC. The rich physics potential of low-x studies at the LHC, especially in the forward region, is discussed and some benchmark measurements in pp, pA and AA collisions are introduced.

PACS. 12.38.-t Quantum chromodynamics – 24.85.+p Quarks, gluons, and QCD in nuclei and nuclear processes – 25.75.-q Relativistic heavy-ion collisions

1 Introduction

1.1 Parton structure and evolution

The partonic structure of the proton (nucleus) can be probed with high precision in deep inelastic scattering (DIS) electron-proton ep (electron-nucleus, eA) collisions. The inclusive DIS hadron cross-section, $\mathrm{d}^2\sigma/\mathrm{d}x\,\mathrm{d}Q^2$, is a function of the virtuality Q^2 of the exchanged gauge boson (*i.e.* its "resolving power"), and the Bjorken-x fraction of the total nucleon momentum carried by the struck parton. The differential cross-section for the neutral-current (γ, Z exchange) process can be written in terms of the target structure functions as

$$\frac{\mathrm{d}^2\sigma}{\mathrm{d}x\,\mathrm{d}Q^2} = \frac{2\pi\alpha^2}{x\,Q^4}\left[Y_+ \cdot F_2 \mp Y_- \cdot xF_3 - y^2 \cdot F_L\right], \quad (1)$$

where $Y_\pm = 1 \pm (1-y)^2$ is related to the collision inelasticity y, and the structure functions $F_{2,3,L}(x,Q^2)$ describe the density of quarks and gluons in the hadron: $F_2 \propto e_q^2\,x\,\Sigma_i(q_i+\bar{q}_i)$, $xF_3 \propto x\,\Sigma_i(q_i-\bar{q}_i)$, $F_L \propto \alpha_s\,xg$ ($xq_i, x\bar{q}_i$ and xg are the corresponding parton distribution functions, PDF). F_2, the dominant contribution to the cross-section over most of phase space, is seen to rise strongly for decreasing Bjorken-x at HERA (fig. 1). The growth in F_2 is well described by $F_2(x,Q^2) \propto x^{-\lambda(Q^2)}$, with $\lambda \approx 0.1$–0.3 logarithmically rising with Q^2 [1]. The F_2 scaling violations evident at small x in fig. 1 are indicative of the increasing gluon radiation from sea quarks. The $xg(x,Q^2)$ distribution itself can be indirectly determined (fig. 2) from the F_2 slope:

$$\frac{\partial F_2(x,Q^2)}{\partial \ln(Q^2)} \approx \frac{10\,\alpha_s(Q^2)}{27\pi}\,xg(x,Q^2). \quad (2)$$
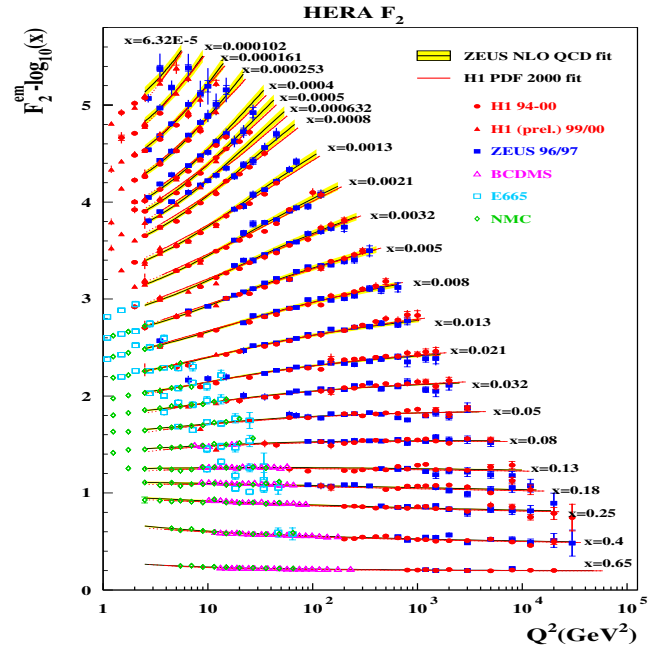
^{a} e-mail: `dde@cern.ch`

Fig. 1. $F_2(x,Q^2)$ measured in proton DIS at HERA ($\sqrt{s} = 320\,\mathrm{GeV}$) and fixed-target ($\sqrt{s} \approx 10$–$30\,\mathrm{GeV}$) experiments.

Although the PDFs are non-perturbative objects obtained from fits to the DIS data, once measured at an input scale $Q_0^2 \gtrsim 2\,\mathrm{GeV}^2$ their value at any other Q^2 can be determined with the Dokshitzer-Gribov-Lipatov-Altarelli-Parisi (DGLAP) evolution equations which govern the probability of parton branchings (gluon splitting, q,g-strahlung) in QCD [2].

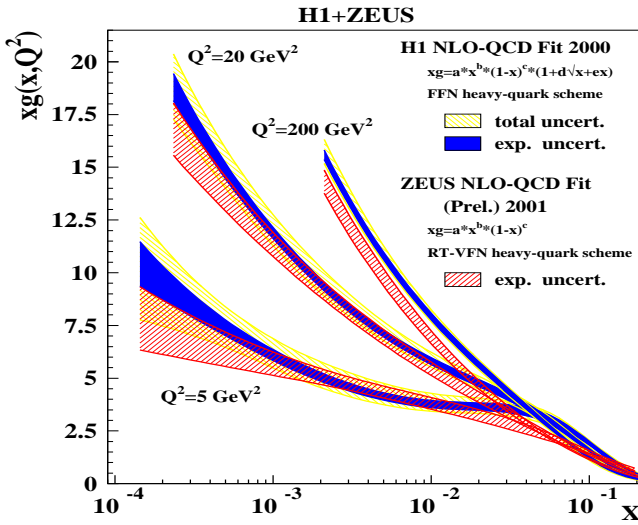The DGLAP parton evolution, however, only takes into account the Q^2-dependence of the PDFs, effectively

Fig. 2. Gluon distributions extracted at HERA (H1 and ZEUS) as a function of x in three bins of Q^2 [3].

Fig. 3. QCD "phase diagram" in the $1/x, Q^2$ plane (each dot represents a parton with transverse area $\sim 1/Q^2$ and fraction x of the hadron momentum). The different evolution regimes (DGLAP, BFKL, saturation) as well as the "saturation scale" and "geometric scaling" curves between the dense and dilute domains are indicated. Adapted from [8].

summing leading powers of $[\alpha_s \ln(Q^2)]^n$ ("leading twist") generated by parton cascades in a region of phase space where the gluons have strongly ordered transverse momenta towards the hard subcollision $Q^2 \gg k_{nT}^2 \gg \cdots \gg k_{1T}^2$. Such a resummation is appropriate when $\ln(Q^2)$ is much larger than $\ln(1/x)$. For decreasing x, the probability of emitting an extra gluon increases as $\propto \alpha_s \ln(1/x)$. In this regime, the evolution of parton densities proceeds over a large rapidity region, $\Delta y \sim \ln(1/x)$, and the finite transverse momenta of the partons become increasingly important. Here the full k_T phase space of the gluons (including scattering of off-shell partons) has to be taken into account and not just the strongly ordered DGLAP part. Thus, the appropriate description of the parton distributions is in terms of k_T-*unintegrated* PDFs, $xg(x, Q^2) = \int^{Q^2} \mathrm{d}k_T^2 G(x, k_T^2)$ with $G(x, k_T^2) \sim h(k_T^2)x^{-\lambda}$, described by the Balitski-Fadin-Kuraev-Lipatov (BFKL) equation [4] which governs parton evolution in x at fixed Q^2. Hints of extra BFKL radiation have been recently found at HERA in the enhanced production of forward jets compared to DGLAP expectations [5,6]. At large Q^2, a description resumming over both $\alpha_s \ln(Q^2)$ and $\alpha_s \ln(1/x)$ is given by the Ciafaloni-Catani-Fiorani-Marchesini (CCFM) evolution equation [7].

1.2 Parton saturation and non-linear evolution at low x

As shown in fig. 2, the gluon density rises very fast for decreasing x. Eventually, at some small enough value of x ($\alpha_s \ln(1/x) \gg 1$) the number of gluons is so large that non-linear (gg fusion) effects become important, taming the growth of the parton densities. In such a high-gluon density regime three things are expected to occur: i) the standard DGLAP and BFKL *linear* equations should no longer be applicable since they only account for single parton branchings ($1 \rightarrow 2$ processes) but not for non-linear
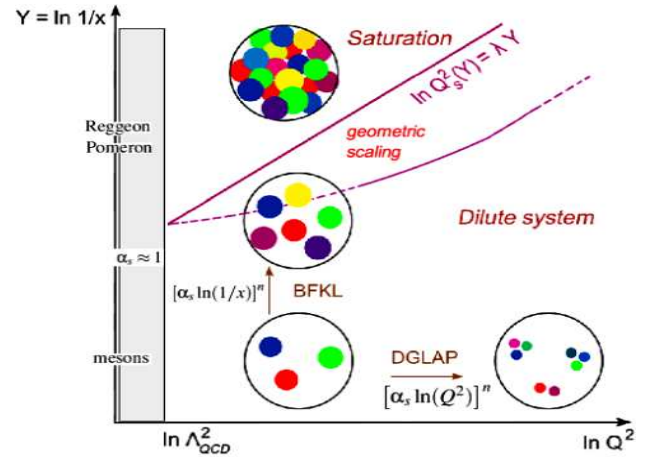
($2 \rightarrow 1$) gluon recombinations; ii) pQCD (collinear and k_T) factorization should break due to its (now invalid) assumption of *incoherent* parton scattering; and, as a result, iii) standard pQCD calculations lead to a *violation of unitarity* even for $Q^2 \gg \Lambda_{QCD}^2$. Figure 3 schematically depicts the different parton evolution regimes as a function of $y = \ln(1/x)$ and Q^2. For small enough x values and for virtualities below an energy-dependent "saturation momentum", Q_s, intrinsic to the *size* of the hadron, one expects to enter the regime of saturated PDFs. Since $xg(x, Q^2)$ can be interpreted as the number of gluons with transverse area $r^2 \sim 1/Q^2$ in the hadron wave function, an increase of Q^2 effectively diminishes the "size" of each parton, partially compensating for the growth in their number (*i.e.* the higher Q^2 is, the smaller the x at which saturation sets in). Saturation effects are, thus, expected to occur when the size occupied by the partons becomes similar to the size of the hadron, πR^2. In the case of nuclear targets with A nucleons (*i.e.* with gluon density $xG = A \cdot xg$), this condition provides a definition for the saturation scale [9, 10]:

$$Q_s^2(x) \simeq \alpha_s \frac{1}{\pi R^2} xG(x, Q^2) \sim A^{1/3} x^{-\lambda}$$
$$\sim A^{1/3}(\sqrt{s})^\lambda \sim A^{1/3} e^{\lambda y}, \tag{3}$$

with $\lambda \approx 0.25$ [11]. Equation (3) tell us that Q_s grows with the number of nucleons in the target and with the energy of the collision, $\sqrt{s}$, or equivalently, the rapidity of the gluon $y = \ln(1/x)$. The nucleon number dependence implies that, at equivalent energies, saturation effects will be enhanced by factors as large as $A^{1/3} \approx 6$ in heavy nuclear targets ($A = 208$ for Pb) compared to protons. In the last fifteen years, an effective field theory of QCD in the high-energy (high density, small x) limit has been developed —the Colour Glass Condensate (CGC) [12]— which describes the hadrons in terms of classical fields (saturated

gluon wave functions) below the saturation scale Q_s. The saturation momentum Q_s introduces a (semi-)hard scale, $Q_s \gg \Lambda_{QCD}$, which not only acts as an infrared cut-off to unitarize the cross-sections but allows weak-coupling perturbative calculations ($\alpha_s(Q_s) \ll 1$) in a strong $F_{\mu\nu}$ colour field background. In the CGC framework, hadronic and nuclear collisions are seen as collisions of classical wave functions which "resum" all gluon recombinations and multiple scatterings. The quantum evolution in the CGC approach is given by the JIMWLK [13] non-linear equations (or by their mean-field limit for $N_c \to \infty$, the Balitsky-Kovchegov equation [14]) which reduce to the standard BFKL kernel at higher x values.

2 Parton saturation: experimental studies

The main source of information on the PDFs is obtained from hard processes as they involve outgoing particles directly coupled to the partonic scattering vertices. Figure 4 summarizes the variety of measurements at different experimental facilities which are sensitive to the gluon density and their approximate x coverage. xG enters directly at LO in hadron-hadron collisions with i) prompt photons, ii) jets, and iii) heavy quarks in the final state, as well as in the (difficult) DIS measurement[1] of iv) the longitudinal structure function F_L. In addition, v) heavy vector mesons ($J/\psi, \Upsilon$) from diffractive photoproduction processes[2] are a valuable probe of the gluon density since their cross-sections are proportional to the *square* of xG [16,17]:

$$\left.\frac{\mathrm{d}\sigma_{\gamma\,p,A\to V\,p,A}}{\mathrm{d}t}\right|_{t=0} = \frac{\alpha_s^2 \Gamma_{ee}}{3\alpha M_V^5} 16\pi^3 \left[xG(x,Q^2)\right]^2, \quad (4)$$

$$\text{with} \quad Q^2 = M_V^2/4 \quad \text{and} \quad x = M_V^2/W_{\gamma\,p,A}^2. \quad (5)$$

The main source of information on the *quark* densities is obtained from measurements of i) the structure functions $F_{2,3}$ in lepton-hadron scattering, and ii) lepton pair (Drell-Yan, DY) production in hadron-hadron collisions. In hadronic collisions, one commonly measures the perturbative probes at central rapidities ($y = 0$), where $x = x_T = Q/\sqrt{s}$, and $Q \sim p_T, M$ is the characteristic scale of the hard scattering. However, one can probe smaller x_2 values in the target by measuring the corresponding cross-sections in the *forward* direction. Indeed, for a $2 \to 2$ parton scattering the *minimum* momentum fraction probed in a process with a particle of momentum p_T produced at pseudo-rapidity η is [18]

$$x_2^{min} = \frac{x_T e^{-\eta}}{2 - x_T e^{\eta}}, \quad \text{where} \quad x_T = 2p_T/\sqrt{s}, \quad (6)$$

---

[1] xG can also be (in)directly extracted from F_2 through the derivative in eq. (2) as well as from the F_2^{charm} data [15].

[2] Diffractive $\gamma\,p$ ($\gamma\,A$) processes are characterized by a quasi-elastic interaction —mediated by a Pomeron or two gluons in a colour singlet state— in which the p (A) remains intact (or in a low excited state) and separated by a rapidity gap from the rest of final-state particles.
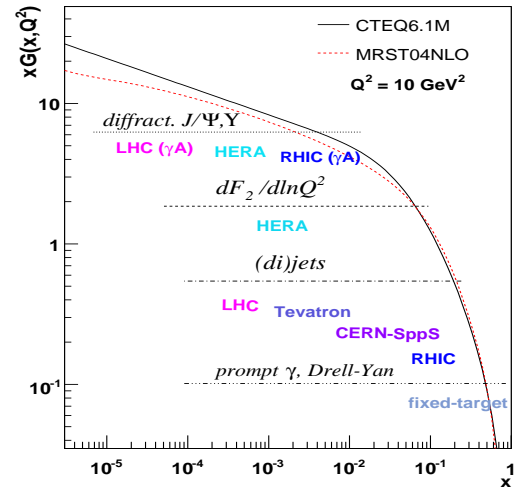

Fig. 4. Examples of experimental measurements at various facilities providing information on the gluon PDF in the range $x \sim 10^{-5}$–0.8.

i.e. x_2^{min} decreases by a factor of ~ 10 every 2 units of rapidity. Though eq. (6) is a lower limit at the end of phase-space (in practice the $\langle x_2 \rangle$ values in parton-parton scatterings are at least 10 larger than x_2^{min} [18]), it provides the right estimate of the typical $x_2 = (p_T/\sqrt{s})\,e^{-\eta}$ values reached in non-linear $2 \to 1$ processes (in which the momentum is balanced by the gluon "medium") as described in parton saturation models [19,20].
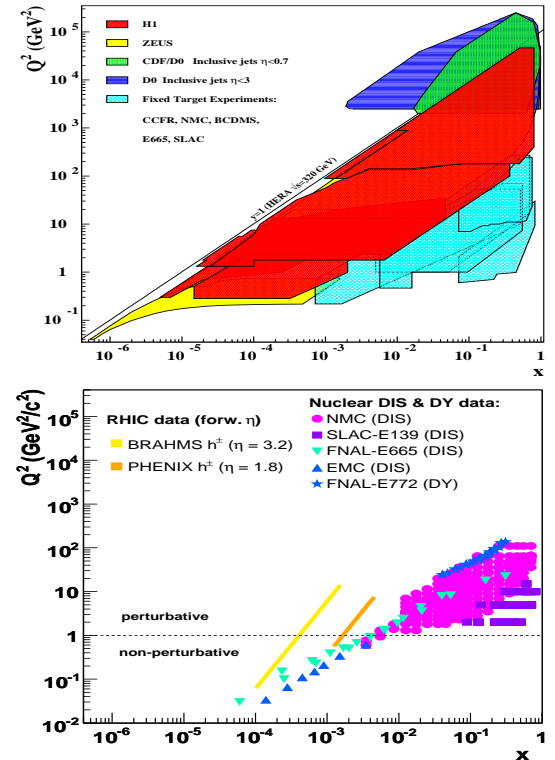

Fig. 5. Available measurements in the (x, Q^2) plane used for the determination of the proton [21] (top) and nuclear [22] (bottom) PDFs.
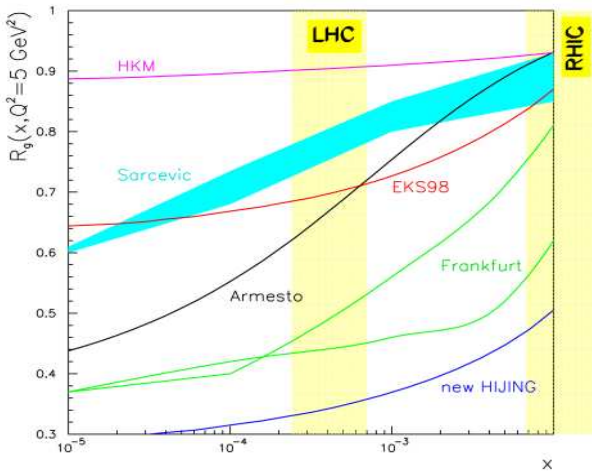
Fig. 6. Ratios of the Pb over proton gluon PDFs *versus* x from different models at $Q^2 = 5\,\text{GeV}^2$. Figure taken from [23].

Figure 5 shows the kinematical map in (x, Q^2) of the existing DIS, DY, direct γ and jet data used in the PDF fits. Results from HERA and the Tevatron cover a substantial range of the proton structure ($10^{-4} \lesssim x \lesssim 0.8$, $1 \lesssim Q^2 \lesssim 10^5\,\text{GeV}^2$) but the available measurements are much rarer in the case of nuclear targets (basically limited to fixed-target studies, $10^{-2} \lesssim x \lesssim 0.8$ and $1 \lesssim Q^2 \lesssim 10^2\,\text{GeV}^2$). As a matter of fact, the nuclear parton distributions are basically unknown at low x ($x < 0.01$) where the only available measurements are fixed-target data in the *non-perturbative* range ($Q^2 < 1\,\text{GeV}^2$) dominated by Regge dynamics rather than quark/gluon degrees of freedom. An example of the current lack of knowledge of the nuclear densities at low x is presented in fig. 6 where different available parametrizations of the ratio of Pb to proton gluon distributions, consistent with the available n DIS data at higher x, show differences as large as a factor of three at $x \sim 10^{-4}$ [23,24].

2.1 HERA results

Though the large majority of ep DIS data collected during the HERA-I phase are successfully reproduced by standard DGLAP predictions, more detailed and advanced experimental and theoretical results in the recent years have pointed to interesting hints of non-linear QCD effects in the data. Arguably, the strongest indication of such effects is given by the so-called "geometric scaling" property observed in inclusive σ_{DIS} for $x < 0.01$ [25] as well as in various diffractive cross sections [26,27]. For inclusive DIS events, this feature manifests itself in a total cross-section at small x ($x < 0.01$) which is only a function of $\tau = Q^2/Q_s^2(x)$, instead of being a function of x and Q^2/Q_s^2 separately (fig. 7). The saturation momentum follows $Q_s(x) = Q_0(x/x_0)^\lambda$ with parameters $\lambda \sim 0.3$, $Q_0 = 1\,\text{GeV}$, and $x_0 \sim 3\cdot 10^{-4}$. Interestingly, the scaling is valid up to very large values of τ, well above the saturation scale, in an "extended scaling" region (see fig. 3), where
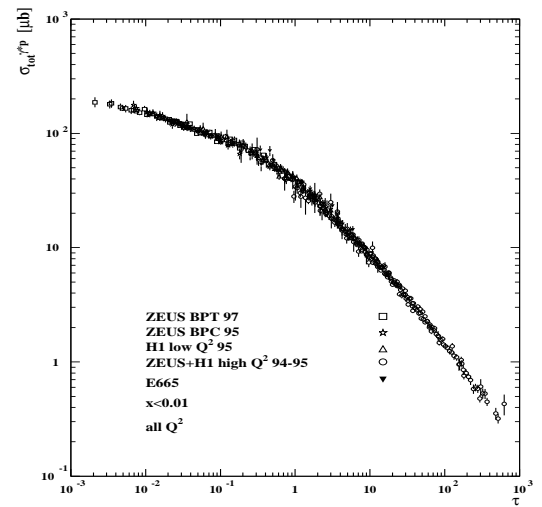

Fig. 7. Geometric scaling in the DIS $\gamma^\star p$ cross-sections plotted *versus* $\tau = Q^2/Q_s^2$ in the range $x < 0.01$, $0.045 < Q^2 < 450\,\text{GeV}^2$ [25].

$Q_s^2 < Q^2 < Q_s^4/\Lambda_{QCD}^2$ [28,8]. The saturation formulation is suitable to describe not only inclusive DIS, but also inclusive diffraction $\gamma^\star p \to X\,p$. The very similar energy dependence of the inclusive diffractive and total cross-sections in $\gamma^\star p$ collisions at a given Q^2 is easily explained in the Golec-Biernat Wüsthoff model [25] but not in standard collinear factorization. Furthermore, geometric scaling has been also found in different diffractive DIS cross-sections (inclusive, vector mesons, deeply-virtual Compton scattering DVCS) [26,27]. All the observed scalings are suggestive manifestations of the QCD saturation regime. Unfortunately, the values of $Q_s^2 \sim 0.5$–$1.0\,\text{GeV}$ at HERA lie in the transition region between the soft and hard sectors and, therefore, non-perturbative effects obscure the obtention of clearcut experimental signatures.

2.2 RHIC results

The expectation of enhanced parton saturation effects in the *nuclear* wave functions accelerated at ultra-relativistic energies, eq. (3), has been one of the primary physics motivations for the heavy-ion programme at RHIC[3] [12]. Furthermore, the properties of the high-density matter produced in the final state of AA interactions cannot be properly interpreted without having isolated first the influence of *initial state* modifications of the nuclear PDFs. After five years of operation, two main experimental results at RHIC have been found consistent with CGC predictions: i) the modest hadron multiplicities measured in AuAu reactions, and ii) the suppressed hadron yield observed at forward rapidities in dAu collisions. (In addition, a recent analysis of the existing nuclear DIS F_2 data also confirms the existence of "geometrical scaling" for $x < 0.017$ [29].)

---

[3] At $y = 0$, the saturation scale for an Au nucleus at RHIC ($Q_s^2 \sim 2\,\text{GeV}$) is larger than that of protons probed at HERA ($Q_s^2 \sim 0.5\,\text{GeV}$).

The bulk hadron multiplicities measured at mid-rapidity in central AuAu at $\sqrt{s_{NN}} = 200\,\text{GeV}$ are $dN_{ch}/d\eta|_{\eta=0} \approx 700$, comparatively lower than the $dN_{ch}/d\eta|_{\eta=0} \approx 1000$ expectations of "minijet" dominated scenarios [30], soft Regge models [31] (without accounting for strong shadowing effects [32]), or extrapolations from an incoherent sum of proton-proton collisions [33]. On the other hand, CGC approaches [11,29] which effectively take into account a reduced number of scattering centers in the nuclear PDFs, $f_{a/A}(x,Q^2) < A \cdot f_{a/N}(x,Q^2)$ reproduce well not only the measured hadron multiplicities but —based on the general expression (3)— also the centrality and c.m. energy dependences of the bulk AA hadron production (fig. 8).

The second manifestation of saturation-like effects in the RHIC data is the BRAHMS observation [34] of suppressed yields of moderately high-p_T hadrons ($p_T \approx 2\text{–}4\,\text{GeV}/c$) in dAu relative to pp collisions at $\eta \approx 3.2$ (fig. 9). Hadron production at such small angles is sensitive to partons in the Au nucleus with $x_2 \approx \mathcal{O}(10^{-3})$. The observed nuclear modification factor, $R_{d\text{Au}} \approx 0.8$, cannot be reproduced by p QCD calculations that include standard *leading-twist* shadowing of the nuclear PDFs [18, 19] but can be described by CGC approaches [36,37] that parametrize the Au nucleus as a saturated gluon wave function. As in the HERA case, it is worth noting however that at RHIC energies the saturation scale is in the transition between the soft and hard regimes ($Q_s^2 \approx 2\,\text{GeV}^2$) and the results consistent with the CGC predictions are in a kinematic range with relatively low momentum scales ($\langle p_T \rangle \sim 0.5\,\text{GeV}$ for the hadron multiplicities and $\langle p_T \rangle \sim 2.5\,\text{GeV}$ for forward inclusive hadron production) where non-perturbative effects can blur a simple interpretation based on partonic degrees of freedom alone.

3 Low-x QCD at the LHC

The Large Hadron Collider (LHC) at CERN will provide pp, pA and AA collisions at $\sqrt{s_{NN}} = 14$, 8.8 and 5.5 TeV, respectively with luminosities $\mathcal{L} \sim 10^{34}$, 10^{29} and $5 \cdot 10^{26}\,\text{cm}^{-2}\,\text{s}^{-1}$. Such large c.m. energies and luminosities will allow detailed QCD studies at unprecedented low x values thanks to the copious production of hard probes (jets, quarkonia, heavy quarks, prompt γ, Drell-Yan pairs, etc.). The advance in the study of low-x QCD phenomena will be specially substantial for nuclear systems since the saturation momentum, eq. (3), $Q_s^2 \approx 5\text{–}10\,\text{GeV}^2$, will be in the perturbative range [11], and the relevant x values, eq. (6), will be 30–70 times lower than AA and pA reactions at RHIC: $x \approx 10^{-3}(10^{-5})$ at central (forward) rapidities for processes with $Q^2 \sim 10\,\text{GeV}^2$ (fig. 10).
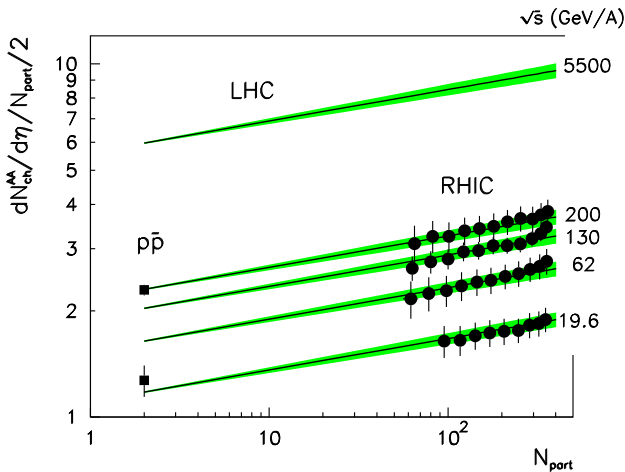

Fig. 8. Dependences on c.m. energy and centrality (given in terms of the number of nucleons participating in the collision, N_{part}) of $dN_{ch}/d\eta|_{\eta=0}$ (normalized by N_{part}): PHOBOS AuAu data [35] *vs.* the predictions of the saturation approach [29].
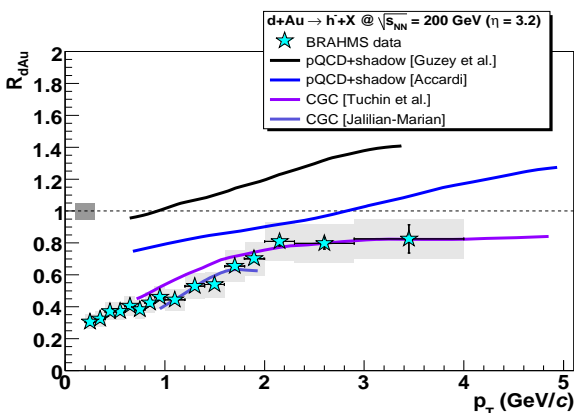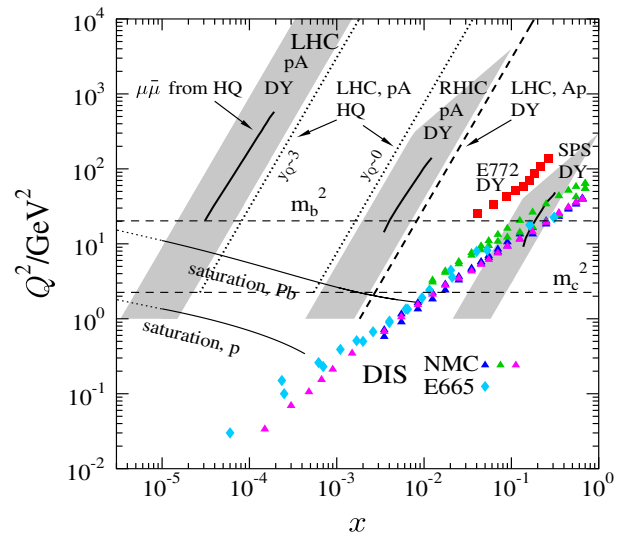

Fig. 9. Nuclear modification factor $R_{d\text{Au}}(p_T)$ for negative hadrons at $\eta = 3.2$ in dAu at $\sqrt{s_{NN}} = 200\,\text{GeV}$: BRAHMS data [34] compared to leading-twist shadowing p QCD [18,19] and CGC [36,37] predictions.

Fig. 10. Kinematical (x, Q^2) range probed at various rapidities y and c.m. energies in $\sqrt{s_{NN}} = 8.8\,\text{TeV}$ pA collisions at the LHC [23].

3.1 The LHC experiments

The four LHC experiments —*i.e.* the two large general-purpose and high-luminosity ATLAS and CMS detector systems as well as the heavy-ion–dedicated ALICE and the heavy-flavour–oriented LHCb experiments— have all detection capabilities in the forward direction very well adapted for the study of low-x QCD phenomena with hard processes in collisions with proton and ion beams:

i) Both CMS and ATLAS feature hadronic calorimeters in the range $3 < |\eta| < 5$ which allow them to measure jet cross-sections at very forward rapidities. Both experiments feature also zero-degree calorimeters (ZDC, $|\eta| \gtrsim 8.5$ for neutrals), which are a basic tool for neutron-tagging "ultra-peripheral" PbPb photoproduction interactions. CMS has an additional electromagnetic/hadronic calorimeter (CASTOR, $5.3 < |\eta| < 6.7$) and shares the interaction point with the TOTEM experiment providing two extra trackers at very forward rapidities (T1, $3.1 < |\eta| < 4.7$, and T2, $5.5 < |\eta| < 6.6$) well-suited for DY measurements.

ii) The ALICE forward muon spectrometer at $2.5 < \eta < 4$, can reconstruct J/ψ and Υ (as well as Z) in the dimuon channel, as well as statistically measure single inclusive heavy-quark production via semileptonic (muon) decays. ALICE counts also on ZDCs in both sides of the interaction point (IP) for forward neutron triggering of PbPb photoproduction processes.

iii) LHCb is a single-arm spectrometer covering rapidities $1.8 < \eta < 4.9$, with very good particle identification capabilities designed to accurately reconstruct b and c mesons. The detector is also well-suited to measure jets, $Q\bar{Q}$ and $Z \to \mu\mu$ production in the forward hemisphere.

3.2 Low-x QCD measurements at LHC

Measurement at the LHC forward rapidities of any of the processes shown in fig. 4 provides an excellent means to look for signatures of high-gluon-density phenomena at low x. Four representative measurements are discussed in the last section of the paper.

– Case study I: forward (di)jets (pp, pA, AA)

The jet measurements in $\bar{p}p$ collisions at Tevatron energies have provide valuable information on the proton PDFs (see fig. 5, top). According to eq. (6), the measurement of jets with $p_T \approx 20$–$200\,\mathrm{GeV}/c$ in pp collisions at $14\,\mathrm{TeV}$ in the ATLAS or CMS forward calorimeters ($3 < |\eta| < 5$) allows one to probe the PDFs at x values as low as $x_2 \approx 10^{-4}$–10^{-5}. Figure 11 shows the actual $\log(x_{1,2})$ distribution of two partons scattering at LHC and producing at least one forward jet as obtained with PYTHIA 6.403 [38]. As expected in forward scattering, the collision is very asymmetric with x_2 (x_1) peaked at $\sim 10^{-4}$ ($\sim 10^{-1}$) and thus provides direct information
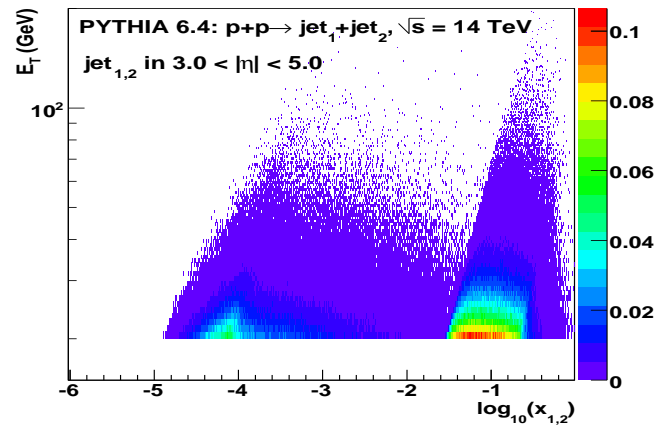

Fig. 11. $\log(x_{1,2})$ distribution of two partons colliding in pp collisions at $\sqrt{s} = 14\,\mathrm{TeV}$ and producing at least one jet within ATLAS/CMS forward calorimeters acceptances as determined with PYTHIA.
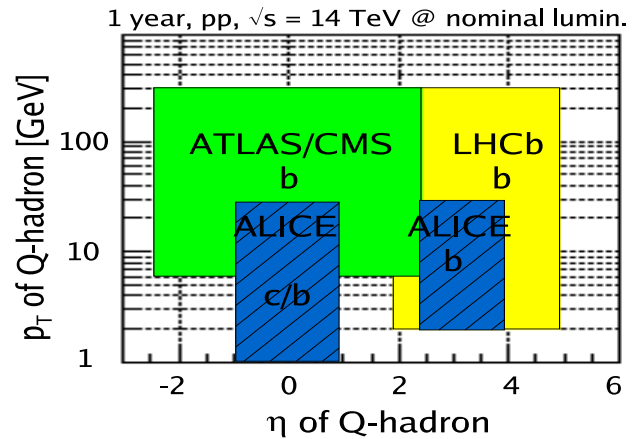

Fig. 12. Acceptances in (η, p_T) for open charm and bottom hadrons in the four LHC experiments for 1-year nominal luminosity [15].

on the low-x parton densities. Not only the single inclusive cross-section but the forward-backward dijet production, "Müller-Navelet jets", is a particularly sensitive measure of BFKL [39] as well as non-linear [6] parton evolutions. In the presence of low-x saturation effects, the Müller-Navelet cross-section for two jets separated by $\Delta\eta \sim 9$ (and, thus, measurable in each one of the forward calorimeters) is expected to be suppressed by a factor of ~ 2 compared to BFKL predictions [6]. A study is underway to determine the feasibility of both forward (di)jet measurements in CMS [40].

– Case study II: forward heavy quarks (pp, pA, AA)

Studies of small-x effects on heavy-flavour production at the LHC in two different approaches, based on collinear and k_T factorization, including non-linear terms in the parton evolution, lead to two different predictions (enhancement *vs.* suppression) for the measured c and b
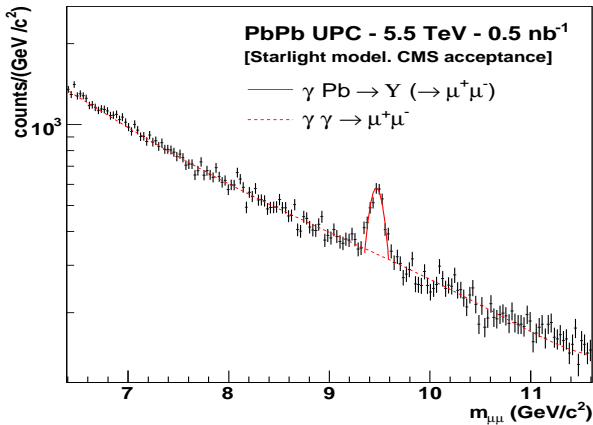
PbPb UPC - 5.5 TeV - 0.5 nb^{-1}
[Starlight model. CMS acceptance]

— $\gamma\,\mathrm{Pb} \to \Upsilon\,(\to \mu^+\mu^-)$
---- $\gamma\,\gamma \to \mu^+\mu^-$

Fig. 13. Expected $\mu^+\mu^-$ invariant mass from $\gamma\,\mathrm{Pb} \to \Upsilon\,\mathrm{Pb}^\star \to \mu^+\mu^-\,\mathrm{Pb}^\star$ and $\gamma\,\gamma \to \mu^+\mu^-$ processes predicted by *Starlight* [44] for UPC PbPb collisions at $\sqrt{s_{NN}} = 5.5\,\mathrm{TeV}$ in the CMS acceptance.

cross-sections [15]. The possibility of ALICE and LHCb to reconstruct D and B mesons in a large rapidity range (fig. 12) will put stringent constraints on the gluon structure and evolution at low-x. In the case of ALICE, the heavy-Q pp studies will have a natural extension in AA and pA collisions [41], providing a precise probe of non-linear effects in the nuclear wave function.

– Case study III: $Q\bar{Q}$ photoproduction (electromagnetic AA)

High-energy diffractive photoproduction of heavy vector mesons $(J/\psi, \Upsilon)$ proceeds through colourless two-gluon exchange (which subsequently couples to $\gamma \to Q\bar{Q}$) and is thus a sensitive probe of the gluon densities at small x, see eq. (4). Ultra-peripheral interactions (UPCs) of high-energy heavy ions generate strong electromagnetic fields which help constrain the low-x behaviour of xG via quarkonia [42], or other hard probes [43], produced in γ-nucleus collisions. Lead beams at 2.75 TeV have Lorentz factors $\gamma = 2930$ leading to maximum (equivalent) photon energies $\omega_{max} \approx \gamma/R \sim 100\,\mathrm{GeV}$, and c.m. energies $W_{\gamma\gamma}^{max} \approx 160\,\mathrm{GeV}$ and $W_{\gamma A}^{max} \approx 1\,\mathrm{TeV}$. From eq. (5), the x values probed in $\gamma A \to J/\psi\,A$ processes at $y = 2$ can be as low as $x \sim 10^{-5}$. The ALICE, ATLAS and CMS experiment can measure $J/\psi, \Upsilon \to e^+e^-, \mu^+\mu^-$ produced in electromagnetic PbPb collisions tagged with neutrons detected in the ZDCs (as done at RHIC [42]). Figure 13 shows the expected dimuon invariant mass distributions around the Υ mass predicted by *Starlight* [44] within the CMS central acceptance ($\eta < 2.5$) for an integrated PbPb luminosity of $0.5\,\mathrm{nb}^{-1}$ [45].

– Case study IV: forward Drell-Yan pairs (pp, pA, AA)

High-mass Drell-Yan pair production at the very forward rapidities covered by LHCb and by the CMS CASTOR and TOTEM T2 detectors can probe the parton densities

down to $x \sim 10^{-6}$ at much higher virtualities M^2 than those accessible in other measurements discussed here. A study is currently underway in CMS [40] to combine the CASTOR electromagnetic energy measurement together with the good position resolution of T2 for charged tracks, to trigger on and reconstruct the e^+e^- invariant mass in pp collisions at 14 TeV, and scrutinize xg in the M^2 and x plane.

4 Conclusion

We have reviewed the physics of non-linear QCD and high gluon densities at small fractional momenta x, with emphasis on the existing data at HERA (proton) and RHIC (nucleus) which support the existence of a parton saturation regime as described, *e.g.*, in the framework of the Colour Glass Condensate effective field theory. The future perspectives at the LHC have been presented, including the promising capabilities of the forward detectors of the ALICE, ATLAS, CMS and LHCb experiments to study the parton densities down to $x \sim 10^{-6}$ with various hard probes (jets, quarkonia, heavy quarks, Drell-Yan). The programme of investigating the dynamics of low-x QCD is not only appealing in its own right but it is an essential prerequisite for predicting a large variety of hadron, photon and neutrino scattering cross-sections at very high energies.

References

1. H1 Collaboration (C. Adloff *et al.*), Phys. Lett. B **520**, 183 (2001).
2. V.N. Gribov, L.N. Lipatov, Sov. J. Nucl. Phys. **15**, 438 (1972); G. Altarelli, G. Parisi, Nucl. Phys. B **126**, 298 (1977); Yu.L. Dokshitzer, Sov. Phys. JETP **46**, 641 (1977).
3. M. Dittmar *et al.*, in *Proceedings of HERA-LHC Workshop*, hep-ph/0511119.
4. L.N. Lipatov, Sov. J. Nucl. Phys. **23**, 338 (1976); E.A. Kuraev, L.N. Lipatov, V.S. Fadin, Zh. Eksp. Teor. Fiz **72**, 3 (1977); Ya.Ya. Balitsky, L.N. Lipatov, Sov. J. Nucl. Phys. **28**, 822 (1978).
5. ZEUS Collaboration (S. Chekanov *et al.*), Phys. Lett. B **632**, 13 (2006); H1 Collaboration (A. Aktas *et al.*), Eur. Phys. J. C **46**, 27 (2006).
6. C. Marquet, C. Royon, Nucl. Phys. B **739**, 131 (2006).
7. S. Catani, F. Fiorani, G. Marchesini, Nucl. Phys. B **336**, 18 (1990); S. Catani, M. Ciafaloni, F. Hautmann, Nucl. Phys. B **366**, 135 (1991).
8. E. Iancu, C. Marquet, G. Soyez, hep-ph/0605174.
9. L. Gribov, E.M. Levin, M.G. Ryskin, Phys. Rep. **100**, 1 (1983).

10. A.H. Mueller, J.-w. Qiu, Nucl. Phys. B **268**, 427 (1986).
11. D. Kharzeev, M. Nardi, Phys. Lett. B **507**, 121 (2001); D. Kharzeev, E. Levin, M. Nardi, Nucl. Phys. A **747**, 609 (2005).
12. See, *e.g.*, E. Iancu, R. Venugopalan, in *QGP*, edited by R.C. Hwa *et al.*, Vol. **3** (World Scientific, Singapore, 2003) hep-ph/0303204; J. Jalilian-Marian, Y.V. Kovchegov, Prog. Part. Nucl. Phys. **56**, 104 (2006) and references therein.
13. J. Jalilian-Marian, A. Kovner, A. Leonidov, H. Weigert, Nucl. Phys. B **504**, 415 (1997); Phys. Rev. D **59**, 014014 (1999); E. Iancu, A. Leonidov, L. McLerran, Nucl. Phys. A **692**, 583 (2001).
14. I. Balitsky, Nucl. Phys. B **463**, 99 (1996); Yu.V. Kovchegov, Phys. Rev. D **61**, 074018 (2000).
15. J. Baines *et al.*, in *Proceedings of HERA-LHC Workshop*, hep-ph/0601164.
16. M.G. Ryskin *et al.*, Z. Phys. C **76**, 231 (1997).
17. T. Teubner, *Proceedings of DIS'05*, AIP Conf. Proc. **792**, 416 (2006).
18. V. Guzey, M. Strikman, W. Vogelsang, Phys. Lett. B **603**, 173 (2004).
19. A. Accardi, Acta Phys. Hung. A **22**, 289 (2005).
20. A. Dumitru, A. Hayashigaki, J. Jalilian-Marian, Nucl. Phys. A **765**, 464 (2006).
21. P. Newman, Int. J. Mod. Phys. A **19**, 1061 (2004).
22. D. d'Enterria, J. Phys. G **30**, S767 (2004).
23. A. Accardi *et al.*, in *Hard probes in Heavy Ion collisions at the LHC*, CERN Yellow report, hep-ph/0308248.
24. N. Armesto, J. Phys. G **32**, R367 (2006).
25. K. Golec-Biernat, M. Wüsthoff, Phys. Rev. D **59**, 014017 (1999); **60**, 114023 (1999).
26. J.R. Forshaw, G. Shaw, JHEP **0412**, 052 (2004).
27. C. Marquet, L. Schoeffel, hep-ph/0606079.
28. E. Iancu, K. Itakura, L. McLerran, Nucl. Phys. A **708**, 327 (2002).
29. N. Armesto, C.A. Salgado, U.A. Wiedemann, Phys. Rev. Lett. **94**, 022002 (2005).
30. M. Gyulassy, X.N. Wang, Comput. Phys. Commun. **83**, 307 (1994).
31. A. Capella, U. Sukhatme, C.I. Tan, Van J. Tran Thanh, Phys. Rep. **236**, 225 (1994).
32. N. Armesto, C. Pajares, Int. J. Mod. Phys. A **15**, 2019 (2000).
33. K.J. Eskola, Nucl. Phys. A **698**, 78 (2002).
34. BRAHMS Collaboration (I. Arsene *et al.*), Nucl. Phys. A **757**, 1 (2005).
35. PHOBOS Collaboration (B.B. Back *et al.*), Nucl. Phys. A **757**, 28 (2005).
36. D. Kharzeev, Y. Kovchegov, K. Tuchin, Phys. Lett. B **599**, 23 (2004).
37. J. Jalilian-Marian, Nucl. Phys. A **748**, 664 (2005).
38. T. Sjostrand, S. Mrenna, P. Skands, JHEP **0605**, 026 (2006).
39. A.H. Mueller, H. Navelet, Nucl. Phys. B **282**, 727 (1987).
40. CMS and TOTEM Collaborations, *Prospects for Diffractive and Forward Physics at LHC*, CERN-LHCC-2006-039/G-124.
41. A. Dainese, *Proceedings of Hard Probes'06*, nucl-ex/0609042.
42. D. d'Enterria, *Proceedings of Quark Matter'05*, nucl-ex/0601001.
43. M. Strikman, R. Vogt, S. White, Phys. Rev. Lett. **96**, 082001 (2006).
44. S.R. Klein, J. Nystrand, Phys. Rev. C **60**, 014903 (1999); A. Baltz, S. Klein, J. Nystrand, Phys. Rev. Lett. **89**, 012301 (2002).
45. CMS Collaboration (D. d'Enterria), Eur. Phys. J. C **49**, 155 (2007).